Decorating Waste Cloth via Industrial Wastewater for Tube-Type Flexible and Wearable Sodium-Ion Batteries

Yun-hai Zhu, Shuang Yuan, Di Bao, Yan-bin Yin, Hai-xia Zhong, Xin-bo Zhang, Jun-min Yan, and Qing Jiang*

Industrial wastewater is one of the major sources of aquatic pollution, which contains various kinds of toxic substances such as cyanides, alkaline cleaning agents, degreasing solvents, oil, fat, as well as metals ions, causing serious problems to both the ecosystem and human health.[1] Among them, nickel (Ni)-containing wastewater has attracted significant attention owing to the huge discharge load and high toxicity to human body.[2] Generally, Ni resources can be treated via various methodologies, including chemical precipitation, ion exchange, adsorption, and electrochemical removal. However, these technologies still suffer from drawbacks such as high cost, complex process, low efficiency, difficulty in separation, and reuse of metal-containing products.[3] On the other hand, due to steady increase of the cotton textile (CT) consumption in the past few decades, vast CT wastes are generated.[4] Like other wastes, textile waste usually are disposed through landfill and incineration, causing serious environment pollution.[5]

Flexible electronics, characterized by lightweight, bendable, rugged, portable, rollable, and potentially foldable, is a burgeoning and promising technology for the next-generation portable electronic devices.[6] In order to realize low-cost and high-performance flexible electronics society, numerous encouraging flexible energy storage prototypes have emerged rapidly, including flexible lithium-ion batteries (LIBs),[7] lithium-O_2 batteries,[8] supercapacitors,[9] and solar cells.[10] Thereinto, flexible rechargeable batteries especially flexible LIBs have been designed successfully. However, there is increasing concern about the cost and limitation of lithium reserves. In response, thanks to the low-cost and widespread geological distribution of sodium resources, it is expected that developing flexible sodium-ion batteries (SIBs) could offer great promise for the next-generation flexible electronics.[11] Although very few inspiriting flexible SIBs have been successfully developed,[12] achieving of good wearability and robustness, especially in conjunction with high energy density, remains a daunting challenge due to the absence of effective components and favorable cell configurations.[13] To the best our knowledge, there are no reports on 1D flexible SIBs, to say nothing of one with tube-shaped structure. Thereafter, developing new strategy to fabricate tube-type flexible SIBs and then exploring its mechanical and electrochemical performances toward practical applications are important while are still very challenging.

Herein, taking laboratory coat waste as a representative example of CT waste, to employ mechanical flexibility/strength and reclaim the valuable metal ions from industrial wastewater, Ni-coated CT (NCT) is fabricated as a flexible current collector using simulated nickel-containing electroless plating wastewater (SNCW)[14] and laboratory coat waste as raw materials. Unexpectedly, the obtained NCT holds many advantages, including high mechanical strength/flexibility, good electronic conductivity, and superior electrochemical stability. Furthermore, as a proof-of-concept application, a binder-free electrode has been successfully fabricated via directly coating the Prussian blue graphene composites on NCT (PB@GO@NCT), which exhibits excellent flexibility and good rate capability (30 C) as well as outstanding cycling stability (up to 1800 cycles). More importantly, for the first time, a novel tube-type flexible SIB with superior electrochemical performance is successfully fabricated. In addition, the tube-type battery allows maximum freedom in the device design, which can speed up the process of flexible electronic commercialization.

The design and fabrication process of NTC are illustrated in **Figure 1**a. Briefly, after the sensitization and activation processes, the lab-gown waste is then immersed in SNCW solution bath[14] for modified electroless nickel plating (MENP). Notably, due to the extreme low Ni ion concentration of SNCW, the bath cannot work via traditional electroless nickel plating protocol. To reuse and reduce the Ni of SNCW quickly and effectively, $NH_3 \cdot H_2O$ and NaH_2PO_2 are introduced, wherein the amount of NaH_2PO_2 should keep a certain concentration, which is crucial for plating process. The MENP process could be visually tracked by the color changes of the SNCW solution (Figure 1b). Compared to the initial SNCW solution (little green), the solution changes to dark blue immediately after adding $NH_3 \cdot H_2O$ and gradually becomes shallow as the plating process going, finally turns to be colorless and transparent after 90 min, possibly as a result of the decreasing concentration of nickel. And inductively coupled plasma atomic emission spectroscopy (ICP-AES) measurements show that the nickel concentration falls rapidly as the increasing of plating time and only ≈3.98 wt% Ni is residuary after plating for 90 min, indicating nearly 98.2% Ni was reduced, thus demonstrating effective purification of the Ni-containing wastewater (Figure 1c). Separation and reuse of obtained metal-containing products is very

Y.-h. Zhu, Y.-b. Yin, Prof. J.-m. Yan, Prof. Q. Jiang
Key Laboratory of Automobile Materials
(Jilin University)
Ministry of Education
Department of Materials Science and Engineering
Jilin University
Changchun 130022, P. R. China
E-mail: junminyan@jlu.edu.cn
Dr. S. Yuan, Dr. D. Bao, H.-x. Zhong, Prof. X.-b. Zhang
State Key Laboratory of Rare Earth Resource Utilization
Changchun Institute of Applied Chemistry
Chinese Academy of Sciences
Changchun 130022, P. R. China

DOI: 10.1002/adma.201603719

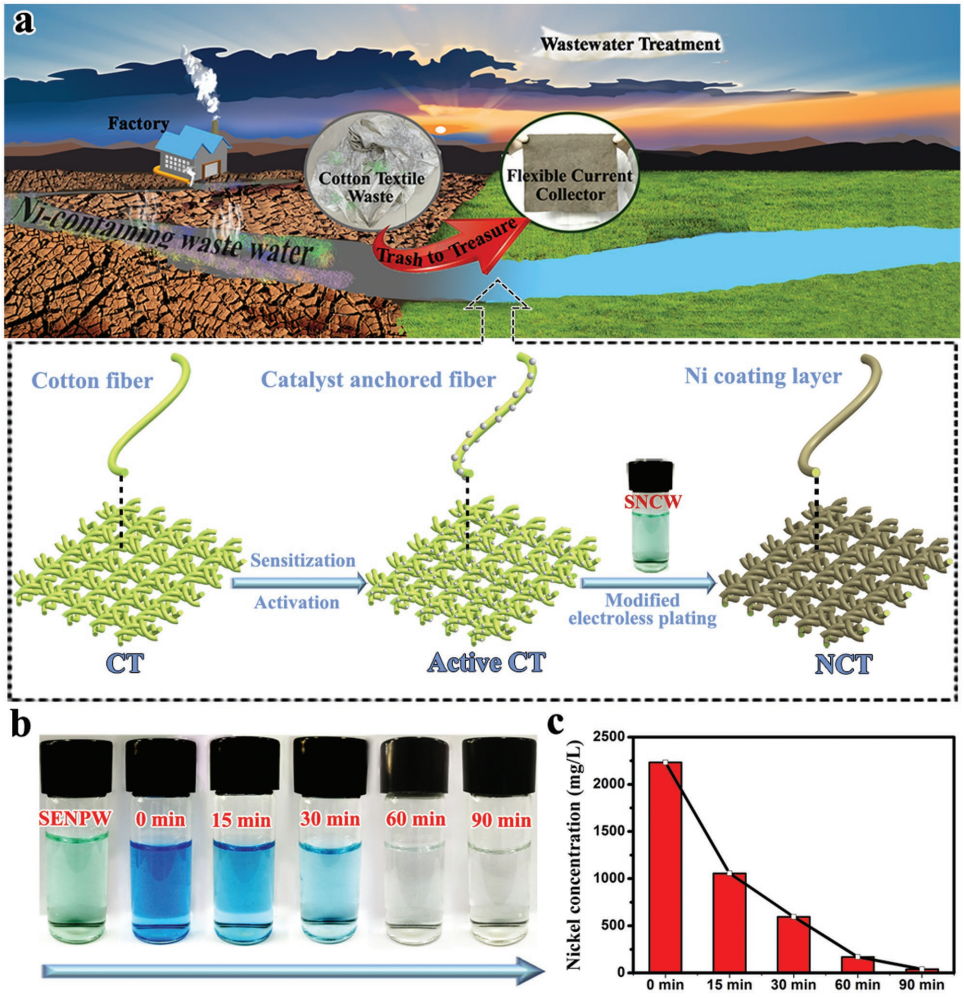

Figure 1. a) Schematic illustration for synthesis of NTC. b) Photographs of SNCW with the color changes over time. c) ICP-AES data of nickel concentration changes over time.

difficult using traditional treatment techniques for industrial wastewater, while it is not a problem using our new strategy.

To investigate the morphology and structure evolution of the NCT, field-emission scanning electron microscopy (FE-SEM) is employed. As shown in Figure S1a,b in the Supporting Information, the bare CT possesses a 3D network structure composed of stacked and intertwined individual smooth cotton fibers. In contrast, the as-synthesized products show a slightly rough surface and larger diameter due to homogeneous coating of Ni layer on the CTs surface (**Figure 2**a–c). Importantly, the 3D network structure has been reserved in NCT, which is in favor of mass transfer.[15] XRD patterns confirm the formation of Ni (Figure S2, Supporting Information), which is further revealed by energy-dispersive X-ray spectrometry (EDS) element mapping (Figure S3, Supporting Information). It should be noted that even distribution of P is also observed in the Ni-coating layer (Figure S3c, Supporting Information), which is likely originated from NaH_2PO_2 during the reduction process. Additionally, X-ray photoelectron spectroscopy (XPS) analysis confirms that the detected P are ascribed to reduced P and PO_4^{3-} species,[16] indicating the successful synthesis of P-doped Ni, which could significantly improve corrosion resistance and the stability of the current collector (Figure S4, Supporting Information).[17]

The excellent mechanical strength of the current collector is crucial to its application in flexible energy storage devices. Figure 2d shows the NCT current collectors could bear ≈48 MPa of stress and its breaking tenacity is nearly ten times that of carbon clothes, thus indicating the as-prepared current collectors are robust enough to keep mechanical integrity upon bending or folding, thus accounting for an excellent cyclability in flexible devices. It is worth noting that the NCT shows higher mechanical strength compared with CT, possibly owing to the potentiation of Ni-coating layer. Furthermore, the electrical conductivity of our prepared NCT reaches a very high level (4900 S m^{-1}), which is much higher than that of most reported flexible conducting materials, including carbon clothes, cotton papers, graphene paper, and carbon nanotube (CNT) conductive textiles (Figure 2e).[18] Interestingly, the NCT also retains good conductivity during the stretch (Figure S5, Supporting Information). More importantly, even after 5000 cycles of bending/stretching (Figure S6, Supporting Information), the electrical

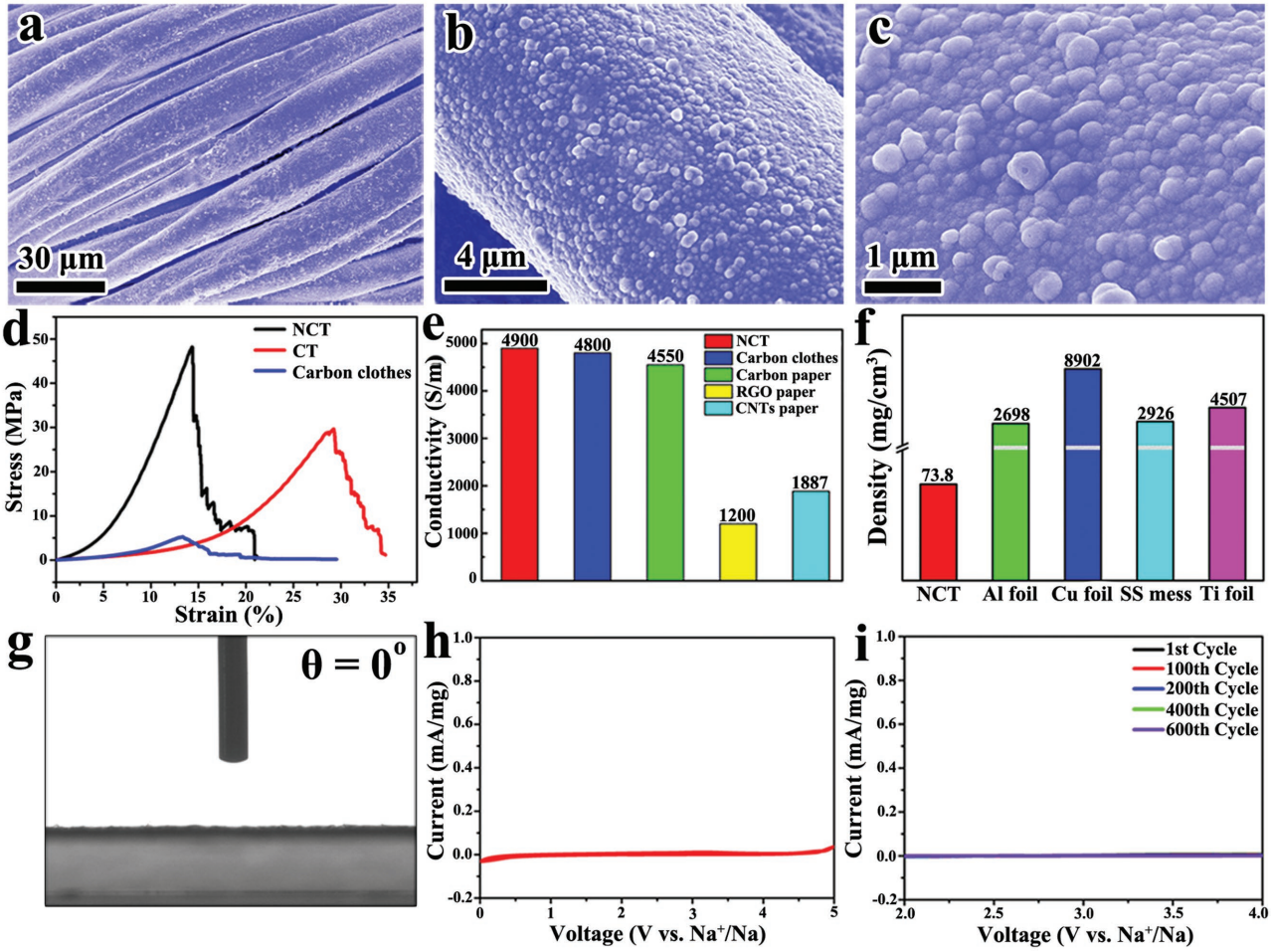

Figure 2. a–c) SEM images of NCT. d) Stress–strain curves of NCT, CT, and carbon clothes. e) Density of NCT and other flexible current collector. f) Electric conductivity of NCT and reported flexible current collectors. g) NMP contact angles image of NCT. h) CV curve of NCT from 0 to 5 V for first cycle. i) Electrochemical stability of NCT from 2 to 4 V.

conductivity of NCT keeps almost unchanged, indicating excellent mechanical stability of NCT. Furthermore, the density of NCT is as low as ≈73.8 mg cm^{-3}, far lower than that of other flexible metal current collector, including Al foil, Cu foil, stainless steel mesh, and Ti foil (Figure 2f). To elucidate the wettability of NCT in organic solvent such as *N*-methyl pyrrolidone (NMP), the contact angle is investigated. As shown in Figure 2g and Figure S7 in the Supporting Information, the contact angles of CT and NCT are both nearly 0°, indicating their excellent wettability and thus demonstrating that the Ni-coating layer would not change the wettability of CT. As another crucial issue of current collectors, the stability of the NCT is verified. The cyclic voltammetry (CV) curve (Figure 2h) shows that NCT is very stable even at 5 V. Additionally, NCT harvests excellent cycling stability with no obvious redox reaction even after 600 cycles (Figure 2i).

Inspired by the attractive properties of NCT, we then apply it as a novel current collector to fabricate a flexible electrode. As a proof-of-concept application, PB is chosen as a representative electrode material. To well integrate individual electroactive particles and avoid using the insulating and electrochemically inactive polymer binders which inevitably reduces the capacity and rate capability,[19] as well as improve the electrical conductivity of PB, graphene oxide is imported to support the PB (PB@GO) in view of the strong adhesion and excellent conductivity of GO. And the formation of PB@GO is confirmed by X-ray diffraction (XRD), transmission electron microscopy (TEM), scanning electron microscopy (SEM), Raman, and thermogravimetric analysis (TGA) (Figure S8–S10, Supporting Information). Typically, PB@GO@NCT integrated binder-free electrodes are obtained by first dispersion of PB@GO composites in NMP and then simply coating on the NCT via a facile dip-coating. Fourier transform infrared spectroscopy and EDS results verify that the PB has been successfully coated on the surface of NCT fibers (Figure S11 and S12, Supporting Information).[20] The SEM images (**Figure 3**a,b) display that the surface of PB@GO@NTC is rougher compared with the bare NCT. Corresponding magnified SEM images indicate that these surfaces are entirely covered by cube-like PB particles, which are connected by GO nanosheets (Figure 3c).

The electrochemical behaviors of the PB@GO@NCT electrodes are evaluated using coin-type cells with sodium metal as counter electrode. Figure 3d displays the CV curves of the PB@GO@NCT electrode between 2 and 4 V at a scan rate

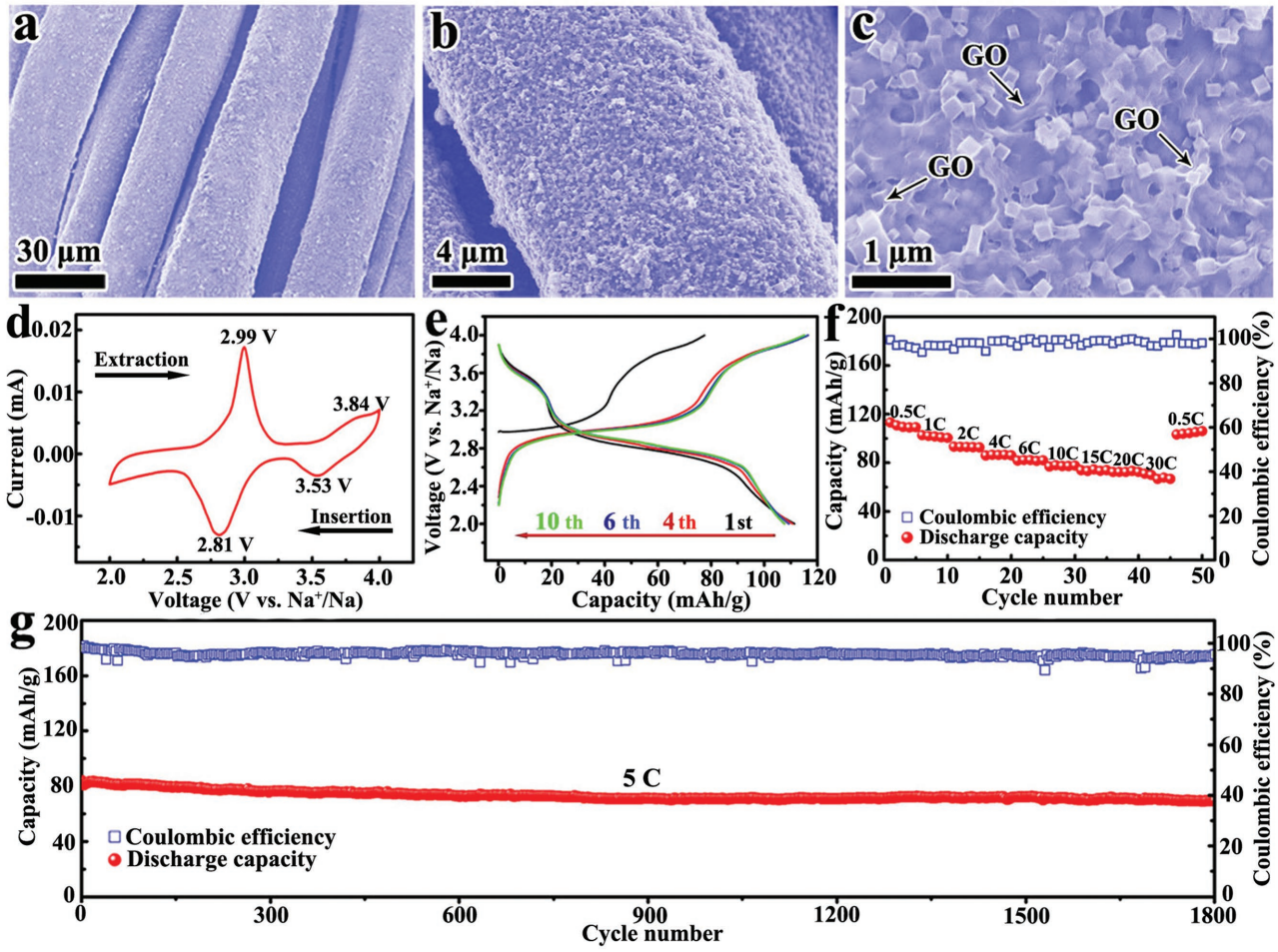

Figure 3. a–c) SEM images, d) CV curves at a scan rate of 0.1 mV s^{-1}, e) galvanostatic charge–discharge profiles at a current density of 0.5 C, f) rate capability at different current densities, and g) cycling performance at a current density of 5 C for PB@GO@NCT integrated electrode (1 C = 120 mA g^{-1}).

of 0.1 mV s^{-1}. The main features in the CV curves appeared as two pairs of well-defined symmetric redox bands locating at 3.84/3.53 V and 2.99/2.81 V, which attributed to oxidation/reduction of the low-spin Fe^{III}/Fe^{II} (coordinated by C atoms) and high-spin Fe^{III}/Fe^{II} couple (coordinated by N atoms), respectively.[21] Figure 3e exhibites the initial ten charge/discharge curves of the as-prepared flexible electrode at a current density of 0.5 C (60 mA g^{-1}). The voltages of the two plateaus are at 2.9 V and 3.8 V on charge, 2.8 and 3.5 V on discharge, which is consistent with the CV results. It should be noted that the initial charge curve is different from the following cycle, possibly as a result of the extraction of potassium ion from the PB during the first charging.[22] In the subsequent cycle, the reversible capacity is maintained at a high capacity of 110 mAh g^{-1} (while the capacity of NCT can be negligible, Figure S14, Supporting Information). Figure 3f shows the rate performance of the PB@GO@NCT cathode at various current densities from 1 to 30 C. The electrode could deliver a discharge capacity of 101, 82, 78, and 72 mA h g^{-1} at rates of 1, 4, 10, and 20 C. Unexpectedly, even at a very high rate of 30 C, the discharge capacity can still reach 67 mA h g^{-1}, corresponding to 61% of its initial reversible capacity. Such a high-rate capability is further affirmed by the charge–discharge curves of PB@GO@NCT at different current densities (Figure S15, Supporting Information). As shown in Figure 3g, the PB@GO@NCT electrode exhibits superior cycling stability, 84.4 % of its initial capacity is maintained even after 1800 cycles at a high rate of 5 C, which corresponds to an extreme small capacity decay of 0.0086% per cycle. The cycling stability at 1 C rate is shown in Figure S16 in the Supporting Information, it also reveals high stability and high columbic efficiency. To the best of our knowledge, PB analogous with such high rate capability and long cycles has been rarely reported (Table S1, Supporting Information). Such a superior electrochemical performance is attributed the structural stability of the PB@GO@NCT (Figure S17, Supporting Information). For comparation, electrodes of PB@GO prepared by traditional method are also investigated. In contrast to the PB@GO@NCT, the PB@GO electrodes show inferior rate and cycle capability (Figure S18, Supporting Information), highlighting the unique 3D conductive network structure and binder-free property of the PB@GO@NCT electrodes.

To demonstrate the application of PB@GO@NTC electrodes in flexible electronics, tube-type flexible SIBs are fabricated. The structure of the flexible battery is demonstrated in **Figure 4**a, composed of a hollow Teflon tube, a copper wire, a metal sodium foil, a flexible separator, a PB@GO@NTC cathode, and

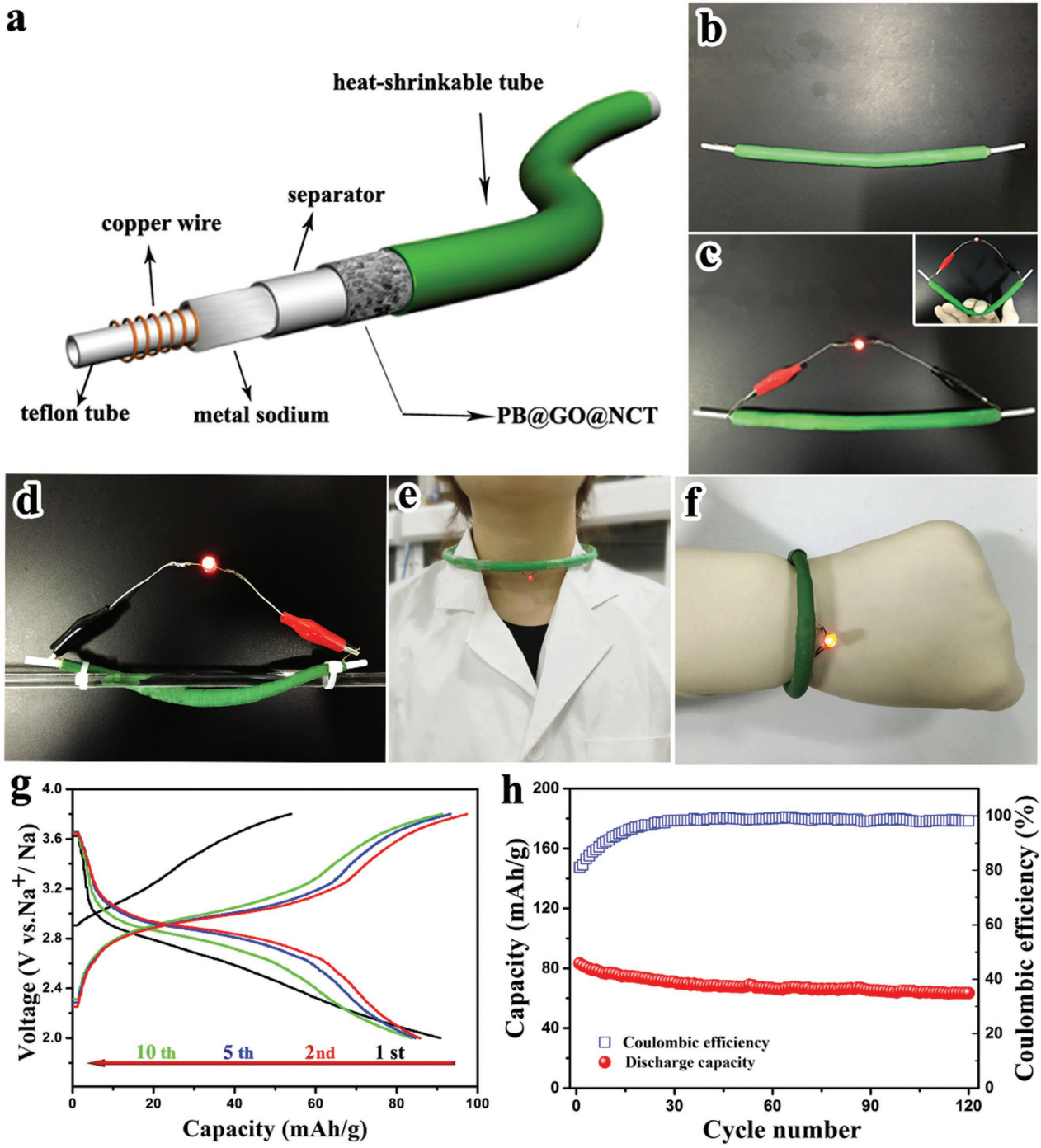

Figure 4. a) Schematic illustration for the structure of the tube-type flexible SIBs. b) Digital photograph of the fabricated tube-type flexible SIBs. c–f) Demonstration of an LED lighting by tube-type flexible SIBs under different conditions. g) Charge–discharge profiles of tube-type flexible SIBs at a current density of 50 mA g^{-1}. h) Cycles performance of tube-type flexible SIBs at a current density of 100 mA g^{-1}.

a shrinkable tube. The Teflon tube inside the battery acts as a support to keep its shape. The shrinkable tube packs the electrode assembly and simultaneously provides sufficient pressure to guarantee a close contact of each battery component. More importantly, PB@GO@NCT electrode, possessed 3D texture structure as well as excellent wettability, could adsorb sufficient electrolyte even under huge pressure during the packing process. Figure 4b displays a photograph of the final packaged tube-type SIBs device, which is consistent well with the schematic in Figure 4a.

To prove its potential application in flexible electronics, the as-fabricated tube-type SIB is used to power a commercial red light-emitting diode (LED). Note that the red LED could be easily lit (Figure 4c), even though the battery is intentionally

bent (inset of Figure 4c) and spiral (Figure 4d). Furthermore, when the tube-type SIBs are processed into various flexible wearable electric devices, including a delicate necklace and compact bracelet, the red LED remains constantly lit (Figure 4e,f). To further demonstrate its application, a watch is also powered by the tube-type flexible SIB (Figure S19b, Supporting Information). Figure 4g shows the initial ten charge/discharge curves of the tube-type SIBs at a current density of 50 mA g^{-1}. The initial discharge capacity is 87 mAh g^{-1}, and the energy density is more than 260 Wh kg^{-1}, which is similar to the button cell. After the first cycle, the discharge capacity is maintained at 83 mAh g^{-1}, demonstrating the excellent stability. Figure 4h shows the cycling performance of the tube-type SIBs at a current density of 100 mA g^{-1}. It reveals that the reversible capacity of the flexible device maintains a nearly constant value of ≈63 mAh g^{-1} and keeps about 76% of its initial capacity even after 120 cycles, demonstrating the excellent capacity retention. Furthermore, to confirm whether the mechanical stress would degrade the electrochemical performance of tube-type flexible SIBs, the discharge performance is compared before and after bending (bending to 30, 60, and 90°; bending hundreds of times); even after bending to 90° (Figure S20a, Supporting Information) or bending hundreds of times (Figure S20b, Supporting Information), the discharge capacities remain almost unchanged, showing high mechanical stability of the tube-type flexible SIBs. Such an excellent performance is attributed to the highly conductive and flexible PB@GO@NTC electrodes.

In summary, to turn waste into treasure, we first develop a facile and cost-effective strategy to effectively revive electroless nickel plating wastewater and the CT waste toward a novel electrode substrate. Unexpectedly, the obtained NCT holds many advantages, in terms of high mechanical strength/flexibility, good electronic conductivity, and superior electrochemical stability. Furthermore, as a proof-of-concept application, a binder-free PB@GO@NTC electrode has been successfully obtained, which exhibits superior electrochemical performance, including high capacity of over 110 mAh g^{-1}, high rate capability of 30 C, and super long life of 1800 cycles. More importantly, for the first time, a novel tube-type flexible and wearable SIB is successfully fabricated, and excellent flexibility, high energy density, and long cycle life are successfully achieved. The proposed strategy, as well as the obtained very promising mechanical and electrochemical performance, would open a new avenue for the treatment and reuse of industrial wastewater and waste cloth toward new value-added applications, which are of great importance to assist the efforts to build a resource sustainable and environment friendly society.

Supporting Information

Supporting Information is available from the Wiley Online Library or from the author.

Acknowledgements

This work was financially supported by National Natural Science Foundation of China (51522101, 51631004, 51471075, and 51401084); National Program on Key Basic Research Project of China (973 Program, Grant Nos. 2012CB215500 and 2014CB932300).

Received: July 13, 2016
Revised: August 19, 2016
Published online: February 23, 2017

[1] a) K. Kadirvelu, K. Thamaraiselvi, C. Namasivayam, *Bioresour. Technol.* **2001**, *76*, 63; b) P. Bautista, A. F. Mohedano, J. A. Casas, J. A. Zazo, J. J. Rodriguez, *J. Chem. Technol. Biotechnol.* **2008**, *83*, 1323; c) E. Erdem, N. Karapinar, R. Donat, *J. Colloid Interface Sci.* **2004**, *280*, 309.
[2] a) K. Periasamy, C. Namasivayam, *Waste Manage.* **1995**, *15*, 63; b) T. Oka, H. Fukazawa, S. Fukui, J. Ogawa, T. Sato, M. Ooizumi, M. Tsujimura, K. Yokoyama, *Phys. C* **2014**, *496*, 58.
[3] a) J. B. Dean, F. L. Bosqui, K. H. Lanouette, *Environ. Sci. Technol.* **1972**, *6*, 518; b) S. McAnally, L. Benefield, R. B. Reed, *Sep. Sci. Technol.* **1984**, *19*, 191; c) R. Nilsson, *Water Res.* **1971**, *5*, 51; d) M. A. Barakat, *Arabian J. Chem.* **2011**, *4*, 361.
[4] R. Deliva, X. Wang, N. Byrne, *RSC Adv.* **2014**, *4*, 29094.
[5] S. S. Muthu, Y. Li, J. Y. Hu, Z. Li, *Fibers Polym.* **2012**, *13*, 1065.
[6] a) J. A. Rogers, T. Someya, Y. Huang, *Science* **2010**, *327*, 1603; b) H. Nishide, K. Oyaizu, *Science* **2008**, *319*, 737; c) X. Pu, L. Li, H. Song, C. Du, Z. Zhao, C. Jiang, G. Cao, W. Hu, Z. Wang, *Adv. Mater.* **2015**, *27*, 2472.
[7] a) B. Liu, J. Zhang, X. Wang, G. Chen, D. Chen, C. Zhou, G. Shen, *ACS Nano* **2012**, *12*, 3005; b) H. Lin, W. Weng, J. Ren, L. Qiu, Z. Zhang, P. Chen, X. Chen, J. Deng, Y. Wang, H. Peng, *Adv. Mater.* **2014**, *26*, 1217.
[8] a) Q. C. Liu, J. J. Xu, D. Xu, X. B. Zhang, *Nat. Commun.* **2015**, *6*, 7892; b) Q. C. Liu, L. Li, J. J. Xu, Z. W Chan, D. Xu, Y. B. Yin, X. Y. Yang, T. L, Y. S. Jiang, J. M. Yan, X. B. Zhang, *Adv. Mater.* **2015**, *27*, 8095; c) Y. Zhang, L. Wang, Z. Guo, Y. Xu, Y. Wang, H. Peng, *Angew. Chem., Int. Ed.* **2016**, *55*, 4487.
[9] a) T. Chen, R. Hao, H. Peng, L. Dai, *Angew. Chem., Int. Ed.* **2015**, *54*, 618; b) G. Sun, X. Zhang, R. Lin, J. Yang, H. Zhang, P. Chen, *Angew. Chem., Int. Ed.* **2015**, *127*, 4734.
[10] a) Z. Liu, J. Li, F. Yan, *Adv. Mater.* **2013**, *25*, 4296; b) J. You, Z. Hong, Y. M. Yang, Q. Chen, M. Cai, T.-B. Song, C.-C. Chen, S. Lu, Y. Liu, H. Zhou, Y. Yang, *ACS Nano* **2014**, *8*, 1674.
[11] a) S. Y. Hong, Y. Kim, Y. Park, A. Choi, N. S. Choi, K. T. Lee, *Energy Environ. Sci.* **2013**, *6*, 2067; b) S. W. Kim, D. H. Seo, X. H. Ma, G. Ceder, K. Kang, *Adv. Energy Mater.* **2012**, *2*, 710; c) S. Yuan, X. Huang, D. Ma, H. Wang, F. Meng, X. B. Zhang, *Adv. Mater.* **2014**, *26*, 2284.
[12] a) H. Wang, P. Hu, J. Yang, G. Gong, L. Guo, X. Chen, *Adv. Mater.* **2015**, *27*, 2348; b) W. Zhang, Y. Liu, C. Chen, Z. Li, Y. Huang, X. Hu, *Small* **2015**, *11*, 3822; c) D. Yang, J. Xu, X. Liao, Y. He, H. Liu, Z. Ma, *Chem. Commun.* **2014**, *50*, 13377.
[13] a) R. Sabbah, R. Kizilel, J. Selman, S. Al-Hallaj, *J. Power Sources* **2008**, *182*, 630; b) X. M. Xu, R. He, *J. Power Sources* **2013**, *240*, 33.
[14] a) C. L. Lia, H. X. Zhao, T. Tsuru, D. Zhou, M. Matsumura, *J. Membr. Sci.* **1999**, *157*, 241; b) T. Ookubo, S. Nishihama, K. Yoshizuka, *Solvent Extr. Res. Dev., Jpn.* **2016**, *20*, 149.
[15] a) X. L. Huang, D. Xu, S. Yuan, D. L. Ma, S. Wang, H. Y. Zheng, X. B. Zhang, *Adv. Mater.* **2014**, *26*, 7264; b) L. Zhang, P. Zhu, F. Zhou, W. Zeng, H. Su, G. Li, J. Gao, R. Sun, C. Wong, *ACS Nano* **2016**, *10*, 1273.
[16] a) X. Zhou, Y. Shen, *J. Mater. Sci.* **2014**, *49*, 3755; b) S. Tian, J. Chen, *Fuel Process. Technol.* **2014**, *122*, 120.
[17] a) R. H. Guo, S. X. Jiang, Y. D. Zheng, J. W. Lan, *J. Appl. Polym. Sci.* **2013**, *127*, 4186; b) U. K. Fatema, Y. Gotoh, *J. Coat. Technol. Res.*

2013, *10*, 415; c) J. Sudagar, J. Lian, W. Sha, *J. Alloys Compd.* **2013**, *571*, 183.

[18] a) J. Chen, H. Bi, S. Sun, Y. Tang, W. Zhao, T. Lin, D. Wan, F. Huang, X. Zhou, X. Xie, M. Jiang, *ACS Appl. Mater. Interfaces* **2013**, *5*, 1408; b) B. Fugetsu, E. Sano, M. Sunada, Y. Sambongi, T. Shibuya, X. S. Wang, T. Hiraki, *Carbon* **2008**, *46*, 1253.

[19] a) B. Koo, H. Kim, Y. Cho, K. T. Lee, N. S. Choi, J. Cho, *Angew. Chem., Int. Ed.* **2012**, *51*, 8762; b) I. Kovalenko, B. Zdyrko, A. Magasinski, B. Hertzberg, Z. Milicev, R. Burtovyy, I. Luzinov, G. Yushin, *Science* **2011**, *334*, 75.

[20] a) P. Nie, L. Shen, G. Pang, Y. Zhu, G. Xu, Y. Qing, H. Dou, X. Zhang, *J. Mater. Chem. A* **2015**, *3*, 16590; b) P. J. Kulesza, M. A. Malik, A. Denca, J. Strojek, *Anal. Chem.* **1996**, *68*, 2442.

[21] a) L. Wang, J. Song, R. Qiao, L. A. Wray, M. A. Hossain, Y. D. Chuang, W. Yang, Y. Lu, D. Evans, J. J. Lee, S. Vail, X. Zhao, M. Nishijima, S. Kakimoto, J. B. Goodenough, *J. Am. Chem. Soc.* **2015**, *137*, 2548; b) X. Wu, W. Deng, J. Qian, Y. Cao, X. Ai, H. Yang, *J. Mater. Chem. A* **2013**, *1*, 10130.

[22] a) Y. H. Lu, L. Wang, J. G. Cheng, J. B. Goodenough, *Chem. Commun.* **2012**, *48*, 6544; b) X. P. Wang, C. J. Niu, J. S. Meng, P. Hu, X. M. Xu, X. J. Wei, L. Zhou, K. N. Zhao, W. Luo, M. Y. Yan, L. Q. Mai, *Adv. Energy Mater.* **2015**, *5*, 1500716.